PERGAMON

International Journal of Solids and Structures 40 (2003) 5371–5388

INTERNATIONAL JOURNAL OF SOLIDS and STRUCTURES

www.elsevier.com/locate/ijsolstr

Initial tension in randomly disordered periodic lattices

E.G. Karpov [a,*], N.G. Stephen [b], Wing Kam Liu [a]

[a] *Department of Mechanical Engineering, Northwestern University, 2145 Sheridan Road, Evanston, IL 60208, USA*
[b] *Mechanical Engineering, School of Engineering Sciences, University of Southampton, Highfield, Southampton SO17 1BJ, United Kingdom*

Received 18 October 2002; received in revised form 29 April 2003

Abstract

This paper is concerned with probabilistic analysis of initial member stress in geometrically imperfect regular lattice structures with periodic boundary conditions. Spatial invariance of the corresponding statistical parameters is shown to arise on the Born-von Kármán domains. This allows analytical treatment of the problem, where the parameters of stress distribution are obtained in a closed form. Several benchmark problems with beam- and plate-like lattices are considered, and the results are verified by the direct Monte–Carlo simulations. Behaviour of the standard deviation as a function of lattice repetitive cell number is investigated, and dependence on the lattice structural redundancy is pointed out.

Keywords: Periodic lattice; Repetitive structure; Lack of fit; Initial tension

1. Introduction

The presence of geometrically imperfect members in a lattice structure is almost inevitable in practice. In terms of the static performance, the most undesirable is member length lack of fit due to manufacturer's tolerance or temperature variations. After assembling a statically indeterminate structure with imperfect member lengths, there can arise considerable bar tensions even before applying the external loading. As investigated by Schmidt et al. (1976, 1983), these unknown stresses may even cause the premature buckling of a particular member; this may further lead to overall progressive collapse of the entire assembly at loads well below its theoretical critical design load. Classical structural theory can mislead the designer into assuming that lattice redundancy should guarantee safety and higher performance, since the structure would remain stiff when some of its redundant members failed. Though with redundancy, the degree by which individual members are critical to structural integrity reduces, Schmidt et al. (1976) have shown that a higher degree of statical indeterminacy usually imposes larger initial stresses, which is more likely to

* Corresponding author. Tel.: +1-847-491-7019; fax: +1-847-491-3915.
E-mail addresses: ekarpov@northwestern.edu (E.G. Karpov), ngs@soton.ac.uk (N.G. Stephen), w-liu@northwestern.edu (W. Kam Liu).

0020-7683/$ - see front matter © 2003 Elsevier Ltd. All rights reserved.
doi:10.1016/S0020-7683(03)00290-7

trigger failure, and it may have no effect on stopping the progressive structural collapse. The sudden collapse of Hartford Coliseum, Connecticut, USA, space roof structure in 1978 under one-half of its design load is known to have been caused by these effects (Smith and Epstein, 1980; Thornton and Lew, 1984).

Thus it is very important to take into account initial bar tensions, even though their calculations may require considerable effort. In the earlier works by Schmidt et al. (1976, 1983) and also El-Sheikh (1995, 1997), the authors employed a deterministic approach to investigate the changes in structural performance due to given lack of fit of particular members at known spatial locations. However, with the hundreds of members and joints in realistic lattices, a statistical description of the initial stress problem would be obviously preferable.

The probabilistic approach to the statics of regular lattices remains relatively undeveloped, in contrast to the area of dynamics, where much greater contributions have been made (see, for example, Li and Benaroya, 1992; Langley, 1994; Lin, 1996). A probable reason is the need for involved multi-dimensional distributions to yield the sought probability for the member stress, as depending on a variety of parameters: the members' lengths variance, its positioning within a representative substructure and, what is most crucial, the global spatial location of such a substructure. Due to the complexity of such a probability distribution, the numerical Monte–Carlo simulation has been considered as a better method of its evaluation, rather than analytical study. Affan and Calladine (1989) accomplished such an analysis to obtain approximate distributions for the initial bar tensions in a two-layered space grid, due to given standard deviations in length, from a series of 200 computer simulations.

Since Monte–Carlo techniques are known to be extremely expensive tools for probabilistic structural analysis, a cheap semi-analytical approach is presented in this paper for problems with periodic (Born-von Kármán) boundary conditions. Due to the cyclic symmetry of Born-von Kármán domains, the probability distributions for initial stress appear to be spatially invariant, i.e. independent of the particular locations of typical members in the structure. This drastically simplifies the analysis of large structures and provides the statistical parameters of these distributions in a straightforward way, in terms of the lattice Green's functions (the Green's functions' definitions are given in Sections 2 and 3).

2. Problem statement and background

Consider the following problem definition: there are given deterministic quantities A, E and L (respectively, the cross-section area, Young's modulus and perfect length) of bar members in a regular pin-jointed lattice. Actual member length, however, does not match the perfect geometry, and there is given a probability distribution (same for all members) for the relative lack of fit,

$$\varepsilon = \Delta L/L. \tag{1}$$

ΔL is the difference between the actual and perfect lengths. The distribution for ε is normal, defined by two statistical parameters: mean value μ_ε (logically, $\mu_\varepsilon = 0$) and standard deviation s_ε (this notation is used instead of the conventional σ to avoid confusion with member stresses). One seeks to express analytically the parameters of probability distributions for the initial stresses in lattice members through A, E, L and s_ε. The boundary conditions are periodic, i.e. Born-von Kármán (for detailed description of these boundary conditions, see, for example Keane and Price (1989), and Karpov et al. (2002)).

2.1. Model for geometric imperfections

For modelling geometric imperfections, a probabilistic extension of the method by El-Sheikh (1995, 1997) is accomplished in this paper. Within the approach, the force

$$P = EA\frac{\Delta L}{L} = EA\varepsilon, \tag{2}$$

required to stretch or shorten a disconnected imperfect member for fitting into the ideal geometry is first calculated. Then the self-equilibrated pair of nodal loads P and $-P$ are applied along the member's longitudinal direction to the joints of the ideal lattice that are connected by this member (Fig. 1). Finally, the strain in the disordered lattice is found as

$$\varepsilon^{(\mathrm{d})} = \varepsilon^{(\mathrm{i})} - \varepsilon, \tag{3}$$

where $\varepsilon^{(\mathrm{i})}$ is the strain of this member in the ideal structure under additional loads P.

Remarkably, this method reduces the analysis of an imperfect lattice (free of external loads) to solving the *loaded ideal structure*. As was shown by Karpov et al. (2002), the latter problem can be most efficiently treated with techniques based on the discrete Fourier transform (DFT). We briefly outline these techniques in Section 2.2, and then combine them with El-Sheikh's ideas (2) and (3) in Section 3 to obtain an effective probabilistic approach.

2.2. Discrete Fourier transform solutions for regular lattices

Imposing periodic (Born-von Kármán) boundary conditions is equivalent to formal merging of the opposite edges of the lattice; this eliminates the difference between the boundary and internal nodal locations. These conditions, therefore, emulate cyclic symmetry on periodic domains. The beam- or plate-like lattices become topological rings or toruses, and their stiffness matrices respectively acquire the cyclic or double-cyclic forms:

$$\mathbf{K} = \begin{pmatrix} \mathbf{k}_2 & \mathbf{k}_3 & \mathbf{0} & \mathbf{k}_1 \\ \mathbf{k}_1 & \mathbf{k}_2 & \mathbf{k}_3 & \mathbf{0} \\ \mathbf{0} & \mathbf{k}_1 & \mathbf{k}_2 & \mathbf{k}_3 \\ \mathbf{k}_3 & \mathbf{0} & \mathbf{k}_1 & \mathbf{k}_2 \end{pmatrix}$$

$$\mathbf{K} = \begin{pmatrix} \mathbf{b}_2 & \mathbf{b}_3 & \mathbf{0} & \mathbf{b}_1 & \mathbf{c}_2 & \mathbf{c}_3 & \mathbf{0} & \mathbf{c}_1 & & & & & & & & \mathbf{a}_2 & \mathbf{a}_3 & \mathbf{0} & \mathbf{a}_1 \\ \mathbf{b}_1 & \mathbf{b}_2 & \mathbf{b}_3 & \mathbf{0} & \mathbf{c}_1 & \mathbf{c}_2 & \mathbf{c}_3 & \mathbf{0} & & & & \mathbf{0} & & & & \mathbf{a}_1 & \mathbf{a}_2 & \mathbf{a}_3 & \mathbf{0} \\ \mathbf{0} & \mathbf{b}_1 & \mathbf{b}_2 & \mathbf{b}_3 & \mathbf{0} & \mathbf{c}_1 & \mathbf{c}_2 & \mathbf{c}_3 & & & & & & & & \mathbf{0} & \mathbf{a}_1 & \mathbf{a}_2 & \mathbf{a}_3 \\ \mathbf{b}_3 & \mathbf{0} & \mathbf{b}_1 & \mathbf{b}_2 & \mathbf{c}_3 & \mathbf{0} & \mathbf{c}_1 & \mathbf{c}_2 & & & & & & & & \mathbf{a}_3 & \mathbf{0} & \mathbf{a}_1 & \mathbf{a}_2 \\ \mathbf{a}_2 & \mathbf{a}_3 & \mathbf{0} & \mathbf{a}_1 & \mathbf{b}_2 & \mathbf{b}_3 & \mathbf{0} & \mathbf{b}_1 & \mathbf{c}_2 & \mathbf{c}_3 & \mathbf{0} & \mathbf{c}_1 & & & & & & & \\ \mathbf{a}_1 & \mathbf{a}_2 & \mathbf{a}_3 & \mathbf{0} & \mathbf{b}_1 & \mathbf{b}_2 & \mathbf{b}_3 & \mathbf{0} & \mathbf{c}_1 & \mathbf{c}_2 & \mathbf{c}_3 & \mathbf{0} & & & & & \mathbf{0} & & \\ \mathbf{0} & \mathbf{a}_1 & \mathbf{a}_2 & \mathbf{a}_3 & \mathbf{0} & \mathbf{b}_1 & \mathbf{b}_2 & \mathbf{b}_3 & \mathbf{0} & \mathbf{c}_1 & \mathbf{c}_2 & \mathbf{c}_3 & & & & & & & \\ \mathbf{a}_3 & \mathbf{0} & \mathbf{a}_1 & \mathbf{a}_2 & \mathbf{b}_3 & \mathbf{0} & \mathbf{b}_1 & \mathbf{b}_2 & \mathbf{c}_3 & \mathbf{0} & \mathbf{c}_1 & \mathbf{c}_2 & & & & & & & \\ & & & & \mathbf{a}_2 & \mathbf{a}_3 & \mathbf{0} & \mathbf{a}_1 & \mathbf{b}_2 & \mathbf{b}_3 & \mathbf{0} & \mathbf{b}_1 & \mathbf{c}_2 & \mathbf{c}_3 & \mathbf{0} & \mathbf{c}_1 \\ & & & & \mathbf{a}_1 & \mathbf{a}_2 & \mathbf{a}_3 & \mathbf{0} & \mathbf{b}_1 & \mathbf{b}_2 & \mathbf{b}_3 & \mathbf{0} & \mathbf{c}_1 & \mathbf{c}_2 & \mathbf{c}_3 & \mathbf{0} \\ & & \mathbf{0} & & \mathbf{0} & \mathbf{a}_1 & \mathbf{a}_2 & \mathbf{a}_3 & \mathbf{0} & \mathbf{b}_1 & \mathbf{b}_2 & \mathbf{b}_3 & \mathbf{0} & \mathbf{c}_1 & \mathbf{c}_2 & \mathbf{c}_3 \\ & & & & \mathbf{a}_3 & \mathbf{0} & \mathbf{a}_1 & \mathbf{a}_2 & \mathbf{b}_3 & \mathbf{0} & \mathbf{b}_1 & \mathbf{b}_2 & \mathbf{c}_3 & \mathbf{0} & \mathbf{c}_1 & \mathbf{c}_2 \\ \mathbf{c}_2 & \mathbf{c}_3 & \mathbf{0} & \mathbf{c}_1 & & & & & \mathbf{a}_2 & \mathbf{a}_3 & \mathbf{0} & \mathbf{a}_1 & \mathbf{b}_2 & \mathbf{b}_3 & \mathbf{0} & \mathbf{b}_1 \\ \mathbf{c}_1 & \mathbf{c}_2 & \mathbf{c}_3 & \mathbf{0} & & & & & \mathbf{a}_1 & \mathbf{a}_2 & \mathbf{a}_3 & \mathbf{0} & \mathbf{b}_1 & \mathbf{b}_2 & \mathbf{b}_3 & \mathbf{0} \\ \mathbf{0} & \mathbf{c}_1 & \mathbf{c}_2 & \mathbf{c}_3 & & & \mathbf{0} & & \mathbf{0} & \mathbf{a}_1 & \mathbf{a}_2 & \mathbf{a}_3 & \mathbf{0} & \mathbf{b}_1 & \mathbf{b}_2 & \mathbf{b}_3 \\ \mathbf{c}_3 & \mathbf{0} & \mathbf{c}_1 & \mathbf{c}_2 & & & & & \mathbf{a}_3 & \mathbf{0} & \mathbf{a}_1 & \mathbf{a}_2 & \mathbf{b}_3 & \mathbf{0} & \mathbf{b}_1 & \mathbf{b}_2 \end{pmatrix}. \tag{4}$$

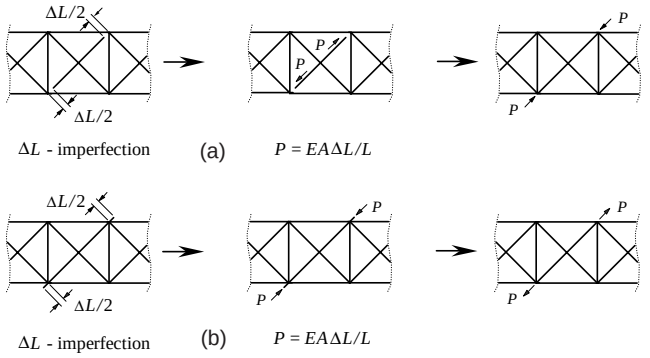

Fig. 1. Modelling of imperfect members by El-Sheikh (1995): short member (a), long member (b).

Generally, the size of blocks **k**, **a**, **b** and **c** is $R \times R$, where R is the number of degrees of freedom for a typical repeating node or set of nodes in the structure. The first matrix, as well as each superblock of the second one (confined by the dashed lines), consists of $N \times N$ blocks, N is the number of repetitive cells in the lattice along the horizontal direction. There are totally $M \times M$ superblocks in the second matrix, where M is the number of cells along the second spatial direction. For example, for the lattice shown in Fig. 4a, $R = 2$ and $N = M = 5$. For the chain of elastic bars, Fig. 3, whose nodes are confined to move along the x-axis only, we have $R = 1$ and $M = 1$. Assuming, for example $N = 4$, and utilising the individual member's stiffness,

$$\mathbf{K}^{(m)} = \frac{EA}{L}\begin{pmatrix} 1 & -1 \\ -1 & 1 \end{pmatrix}, \tag{5}$$

one obtains the cyclic global matrix, as a particular case of the more general form (4):

$$\mathbf{K} = \frac{EA}{L}\begin{pmatrix} 2 & -1 & 0 & -1 \\ -1 & 2 & -1 & 0 \\ 0 & -1 & 2 & -1 \\ -1 & 0 & -1 & 2 \end{pmatrix}. \tag{6}$$

These example structures are discussed in more details in Section 4.

Noteworthy, the maximum number of *distinct* blocks of each type **k**, **a**, **b** or **c**, as well as the number of the distinct superblocks in (4) is three. Thus, the stiffness matrix of a regular beam or plate lattice is comprised respectively of not more than three or nine repeating $R \times R$ blocks, when periodic boundary conditions are applied. Note also that any column or row of the cyclic forms (4) contains all the distinct blocks available. Physically, the diagonal block shows stiffness at a current node with all other nodes being fixed, and the remaining blocks describe the available stiffness couplings between the current and neighbouring nodes.

Both the single- and multi-cyclic systems can be effectively solved by the approach proposed by Karpov et al. (2002). Within this approach, first the *typical nodal location* is defined as a minimum set of nodes able to generate the rest of structural joints, when translated along one (beam lattices) or two (plate lattices) spatial directions. Next, the *associate substructure* is introduced to include all the structural elements interacting with the nodes of one typical location (examples are shown on Figs. 2, 4b and 5b). Importantly, the associate substructure is the minimum structural domain, whose stiffness matrix contains all the distinct blocks available for a global matrix (4).

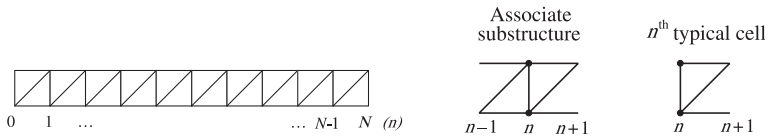

Fig. 2. Substructuring of a beam-like lattice.

Introduce the column-vectors of the generalized loads and displacements **f** and **u**, as related to the degrees of freedom of only one typical nodal location. Then, constructing the associate substructure stiffness matrix, one logically finds the blocks for (4) located along the middle horizontal and vertical lines of the matrix:

$$\begin{pmatrix} \cdots & \mathbf{k}_3 & \cdots \\ \mathbf{k}_1 & \mathbf{k}_2 & \mathbf{k}_3 \\ \cdots & \mathbf{k}_1 & \cdots \end{pmatrix} \begin{pmatrix} \mathbf{u}(n-1) \\ \mathbf{u}(n) \\ \mathbf{u}(n+1) \end{pmatrix} = \begin{pmatrix} \mathbf{f}(n-1) \\ \mathbf{f}(n) \\ \mathbf{f}(n+1) \end{pmatrix} \tag{7}$$

for a one-dimensional beam-like structure, or

$$\begin{pmatrix} & & & & \mathbf{c}_3 & & & & \\ & & & & \mathbf{c}_2 & & & & \\ & & \cdots & & \mathbf{c}_1 & & \cdots & & \\ & & & & \mathbf{b}_3 & & & & \\ \mathbf{a}_1 & \mathbf{a}_2 & \mathbf{a}_3 & \mathbf{b}_1 & \mathbf{b}_2 & \mathbf{b}_3 & \mathbf{c}_1 & \mathbf{c}_2 & \mathbf{c}_3 \\ & & & & \mathbf{b}_1 & & & & \\ & & \cdots & & \mathbf{a}_3 & & \cdots & & \\ & & & & \mathbf{a}_2 & & & & \\ & & & & \mathbf{a}_1 & & & & \end{pmatrix} \begin{pmatrix} \mathbf{u}(n-1,m-1) \\ \mathbf{u}(n,m-1) \\ \mathbf{u}(n+1,m-1) \\ \mathbf{u}(n-1,m) \\ \mathbf{u}(n,m) \\ \mathbf{u}(n+1,m) \\ \mathbf{u}(n-1,m+1) \\ \mathbf{u}(n,m+1) \\ \mathbf{u}(n+1,m+1) \end{pmatrix} = \begin{pmatrix} \mathbf{f}(n-1,m-1) \\ \mathbf{f}(n,m-1) \\ \mathbf{f}(n+1,m-1) \\ \mathbf{f}(n-1,m) \\ \mathbf{f}(n,m) \\ \mathbf{f}(n+1,m) \\ \mathbf{f}(n-1,m+1) \\ \mathbf{f}(n,m+1) \\ \mathbf{f}(n+1,m+1) \end{pmatrix} \tag{8}$$

for plate-like lattices.

Next consider the beam- and plate-like cases separately. For the purposes of further discussion, introduce the following notations for the matrix blocks of (7):

$$\mathbf{K}(1) = \mathbf{k}_1, \quad \mathbf{K}(0) = \mathbf{k}_2, \quad \mathbf{K}(-1) = \mathbf{k}_3. \tag{9}$$

According to (7) and (9), the external loads applied to any nth nodal location will be in equilibrium with structural reaction, if

$$\mathbf{K}(1)\mathbf{u}(n-1) + \mathbf{K}(0)\mathbf{u}(n) + \mathbf{K}(-1)\mathbf{u}(n+1) = \mathbf{f}(n), \quad n = 0, 1, \ldots, N-1. \tag{10}$$

This second order finite difference scheme represents the governing equation of static equilibrium of a repetitive beam-like lattice on an N-periodic domain. It can be reduced to the *discrete convolution* form

$$\sum_{n'=n-1}^{n+1} \mathbf{K}(n-n')\mathbf{u}(n') = \mathbf{f}(n), \quad n = 0, 1, \ldots, N-1, \tag{11}$$

where $\mathbf{K}(n)$ acquires the sense of a stiffness kernel function, whose values are available from (7); $\mathbf{u}(n)$ is the sought displacement function, and function $\mathbf{f}(n)$ describes the external loads distribution.

Using the formal N-periodic extension for the displacement, load and kernel functions,

$$\mathbf{u}(n+vN) = \mathbf{u}(n), \quad \mathbf{f}(n+vN) = \mathbf{f}(n), \quad \mathbf{K}(n+vN) = \mathbf{K}(n), \ v = 0, \pm 1, \pm 2, \ldots, \tag{12}$$

and applying the finite discrete Fourier transform to both sides of equation (11)

$$\sum_{n=0}^{N-1}\sum_{n'=n-1}^{n+1}\mathbf{K}(n-n')\mathbf{u}(n')\exp\Big(-\mathrm{i}2\pi p\frac{n}{N}\Big)=\sum_{n=0}^{N-1}\mathbf{f}(n)\exp\Big(-\mathrm{i}2\pi p\frac{n}{N}\Big), \tag{13}$$

one obtains a set of N decoupled $R\times R$ matrix equations in the Fourier domain:

$$\widetilde{\mathbf{K}}(p)\tilde{\mathbf{d}}(p)=\tilde{\mathbf{f}}(p),\quad p=0,1,\ldots,N-1. \tag{14}$$

Here, the Fourier images of functions (12) read

$$\begin{aligned}\tilde{\mathbf{u}}(p)&=\sum_{n=0}^{N-1}\mathbf{d}(n)\exp\Big(-\mathrm{i}2\pi p\frac{n}{N}\Big),\\ \tilde{\mathbf{f}}(p)&=\sum_{n=0}^{N-1}\mathbf{f}(n)\exp\Big(-\mathrm{i}2\pi p\frac{n}{N}\Big),\\ \widetilde{\mathbf{K}}(p)&=\sum_{n=-1}^{1}\mathbf{K}(n)\exp\Big(-\mathrm{i}2\pi p\frac{n}{N}\Big).\end{aligned} \tag{15}$$

Further inversion of matrix $\widetilde{\mathbf{K}}(p)$, which can be often accomplished symbolically, and application of the inverse DFT yields the sought n-domain solution:

$$\mathbf{u}(n)=\frac{1}{N}\sum_{p=0}^{N-1}\widetilde{\mathbf{K}}^{-1}(p)\tilde{\mathbf{f}}(p)\exp\Big(\mathrm{i}2\pi p\frac{n}{N}\Big). \tag{16}$$

Substitute the Fourier image $\tilde{\mathbf{f}}(p)$ into (16), employing $n=n'$ for (15) to distinguish the summation index there from the argument of function $\mathbf{u}(n)$, and rearrange to give

$$\mathbf{u}(n)=\frac{1}{N}\sum_{p=0}^{N-1}\widetilde{\mathbf{K}}^{-1}(p)\sum_{n'=0}^{N-1}\mathbf{f}(n')\exp\Big(-\mathrm{i}2\pi p\frac{n'}{N}\Big)\exp\Big(\mathrm{i}2\pi p\frac{n}{N}\Big)=\sum_{n'=0}^{N-1}\mathbf{G}_N(n-n')\mathbf{f}(n'), \tag{17}$$

$$\mathbf{G}_N(n)=\frac{1}{N}\sum_{p=0}^{N}\widetilde{\mathbf{K}}^{-1}(p)\exp\Big(\mathrm{i}2\pi p\frac{n}{N}\Big). \tag{18}$$

In fact, matrix $\widetilde{\mathbf{K}}(p)$ appears to be singular for $p=0$, therefore equation $\widetilde{\mathbf{K}}(0)\tilde{\mathbf{d}}(0)=\tilde{\mathbf{f}}(0)$ is solved separately to give the following correction to (18)

$$\mathbf{G}_N(n)=\frac{1}{N}\sum_{p=0}^{N-1}\widetilde{\mathbf{G}}_N(p)\exp\Big(\mathrm{i}2\pi p\frac{n}{N}\Big),\quad \widetilde{\mathbf{G}}_N(p)=\begin{cases}\widetilde{\mathbf{K}}^{-1}(p), & p>0,\\ \mathbf{W}\boldsymbol{\Lambda}^{-1}\mathbf{W}^{+}, & p=0.\end{cases} \tag{19}$$

Here, the diagonal matrix Λ is comprised of non-zero eigenvalues of $\widetilde{\mathbf{K}}(0)$, and the columns of rectangular matrix $\mathbf{W}$ are the corresponding eigenvectors; $\mathbf{W}^{+}$ is the pseudoinverse of $\mathbf{W}$. In case of a zero matrix $\widetilde{\mathbf{K}}(0)$, one assumes $\widetilde{\mathbf{G}}_N(0)=\mathbf{0}$. Matrix function (19) is the displacement *Green's function* for Eq. (11) on the cyclic N-periodic domain. The convolution sum (17) over the Green's and the load functions gives a particular non-homogeneous solution to (11) to describe the lattice deflections precise up to a rigid-body motion.

The *physical interpretation* of the displacement Green's function, according to (17), is that the rth column of $\mathbf{G}_N(n-n')$ represents deflections of the nth nodal set caused by the rth component of a unit load vector applied to the n'th nodal location of a repetitive framework, which is formally closed to form the N-periodic ring. Obviously, the Green's function is defined by the member stiffnesses and lattice geometry only.

The two-dimensional (plate-like) extension of the above approach can be accomplished by denoting the blocks of (8) as

$$\begin{aligned}
&\mathbf{K}(1,1)=\mathbf{a}_1, \quad \mathbf{K}(0,1)=\mathbf{a}_2, \quad \mathbf{K}(-1,1)=\mathbf{a}_3,\\
&\mathbf{K}(1,0)=\mathbf{b}_1, \quad \mathbf{K}(0,0)=\mathbf{b}_2, \quad \mathbf{K}(-1,0)=\mathbf{b}_3,\\
&\mathbf{K}(1,-1)=\mathbf{c}_1, \quad \mathbf{K}(0,-1)=\mathbf{c}_2, \quad \mathbf{K}(-1,-1)=\mathbf{c}_3,
\end{aligned} \tag{20}$$

and writing the governing double convolution form:

$$\sum_{n'=n-1}^{n+1}\sum_{m'=m-1}^{m+1}\mathbf{K}(n-n',m-m')\mathbf{u}(n',m')=\mathbf{f}(n,m), \quad n=1,2,\ldots,N-1,\ m=1,2,\ldots,M-1. \tag{21}$$

Solution to (21) can be similarly obtained in terms of the two-dimensional (N,M)-periodic Green's function with the use of double discrete Fourier transform:

$$\mathbf{u}(n,m)=\sum_{n'=0}^{N-1}\sum_{m'=0}^{M-1}\mathbf{G}_{N,M}(n-n',m-m')\mathbf{f}(n',m'), \tag{22}$$

$$\mathbf{G}_{N,M}(n,m)=\frac{1}{NM}\sum_{p=0}^{N-1}\sum_{q=0}^{M-1}\widetilde{\mathbf{G}}_{N,M}(p,q)\exp\left(\mathrm{i}2\pi\left(p\frac{n}{N}+q\frac{m}{M}\right)\right), \tag{23}$$

$$\begin{aligned}
&\widetilde{\mathbf{G}}_{N,M}(p,q)=\begin{cases}\widetilde{\mathbf{K}}^{-1}(p,q), & p+q>0,\\ \mathbf{W}\mathbf{\Lambda}^{-1}\mathbf{W}^{+}, & p=q=0,\end{cases}\\
&\widetilde{\mathbf{K}}(p,q)=\sum_{n=-1}^{1}\sum_{m=-1}^{1}\mathbf{K}(n,m)\exp\left(-\mathrm{i}2\pi\left(p\frac{n}{N}+q\frac{m}{M}\right)\right).
\end{aligned} \tag{24}$$

Here, matrices $\mathbf{\Lambda}$ and $\mathbf{W}$ of (24) are constructed from the non-zero eigenvalues and the corresponding eigenvectors of $\widetilde{\mathbf{K}}(0,0)$; if $\widetilde{\mathbf{K}}(0,0)=\mathbf{0}$, then $\widetilde{\mathbf{G}}_{N,M}(0,0)=\mathbf{0}$.

3. Spatial invariance of statistics

3.1. Beam-like problem

Return to the original problem definition (the first paragraph of Section 2), and consider first the case of beam-like lattices. Isolate mentally a minimum set of typical bar members the *typical cell* (an example is shown on Fig. 2), numbered with a single spatial parameter n, and introduce the following subsidiary objects, which depend on the value n:

$$\begin{aligned}
&\boldsymbol{\sigma}(n)=\begin{pmatrix}\sigma_1(n)\\ \sigma_2(n)\\ \ldots\end{pmatrix}, \quad \varepsilon(n)=\begin{pmatrix}\varepsilon_1(n)\\ \varepsilon_2(n)\\ \ldots\end{pmatrix}, \quad \varepsilon^{(\mathrm{i})}(n)=\begin{pmatrix}\varepsilon_1^{(\mathrm{i})}(n)\\ \varepsilon_2^{(\mathrm{i})}(n)\\ \ldots\end{pmatrix},\\
&\mathbf{L}(n)\equiv\mathbf{L}=\begin{pmatrix}L_1 & 0 & \ldots\\ 0 & L_2 & \ldots\\ \ldots & \ldots & \ldots\end{pmatrix}, \quad \mathbf{A}(n)\equiv\mathbf{A}=\begin{pmatrix}A_1 & 0 & \ldots\\ 0 & A_2 & \ldots\\ \ldots & \ldots & \ldots\end{pmatrix}, \quad n=0,1,\ldots,N-1.
\end{aligned} \tag{25}$$

Here, $\sigma_k(n)$, $\varepsilon_k(n)$, $\varepsilon_k^{(\mathrm{i})}(n)$, L_k, A_k are the stress, relative lack of fit, strain in the ideal lattice, perfect length and cross-sectional area of the kth member in the nth typical cell, respectively. The Young's modulus is supposed to be the same throughout the lattice.

Assume also that there is known the connectivity matrix $\boldsymbol{\beta}$ for the typical cell with ideal geometry. This matrix relates member elongations and nodal displacements, therefore

$$\mathbf{L}\varepsilon^{(\mathrm{i})}(n) = \boldsymbol{\beta}\begin{pmatrix} \mathbf{d}(n) \\ \mathbf{d}(n+1) \end{pmatrix} \tag{26}$$

for any n within the perfect lattice.

Further consider a particular realization of the random lack of fit $\boldsymbol{\varepsilon}(n)$ for all components of this vector and for all $n = 0, 1, \ldots, N-1$. Then, the ideal lattice is to be subjected to the corresponding nodal loads that can be written, for this realization, in terms of the above notations as

$$\begin{pmatrix} \mathbf{f}(n) \\ \mathbf{f}(n+1) \end{pmatrix} = E\boldsymbol{\alpha}\mathbf{A}\boldsymbol{\varepsilon}(n), \tag{27}$$

where $\boldsymbol{\alpha}$ is the equilibrium matrix for the typical cell, relating the nodal and member forces (2). Note, the equilibrium and connectivity matrices are related as

$$\boldsymbol{\alpha}^{\mathrm{T}} = \boldsymbol{\beta}. \tag{28}$$

According to (17), the displacements for (26) caused by the loads (27) are

$$\begin{aligned} \mathbf{d}(n) &= \sum_{n'=0}^{N-1} (\mathbf{G}_N(n-n')\mathbf{f}(n') + \mathbf{G}_N(n-1-n')\mathbf{f}(n'+1)), \\ \mathbf{d}(n+1) &= \sum_{n'=0}^{N-1} (\mathbf{G}_N(n+1-n')\mathbf{f}(n') + \mathbf{G}_N(n-n')\mathbf{f}(n'+1)). \end{aligned} \tag{29}$$

By rearranging (29) to a matrix form and subsequently employing (27) and (28), we obtain

$$\begin{aligned} \begin{pmatrix} \mathbf{d}(n) \\ \mathbf{d}(n+1) \end{pmatrix} &= \sum_{n'=0}^{N-1} \begin{pmatrix} \mathbf{G}_N(n-n') & \mathbf{G}_N(n-1-n') \\ \mathbf{G}_N(n+1-n') & \mathbf{G}_N(n-n') \end{pmatrix} \begin{pmatrix} \mathbf{f}(n') \\ \mathbf{f}(n'+1) \end{pmatrix} \\ &= E\sum_{n'=0}^{N-1} \begin{pmatrix} \mathbf{G}_N(n-n') & \mathbf{G}_N(n-1-n') \\ \mathbf{G}_N(n+1-n') & \mathbf{G}_N(n-n') \end{pmatrix} \boldsymbol{\beta}^{\mathrm{T}}\mathbf{A}\boldsymbol{\varepsilon}(n'). \end{aligned} \tag{30}$$

Thus, the strains $\varepsilon^{(\mathrm{i})}(n)$ in an ideal lattice can be expressed through the displacement Green's function, according to (26) and (30):

$$\boldsymbol{\varepsilon}^{(\mathrm{i})}(n) = \mathbf{L}^{-1}\boldsymbol{\beta}\begin{pmatrix} \mathbf{d}(n) \\ \mathbf{d}(n+1) \end{pmatrix} = E\mathbf{L}^{-1}\boldsymbol{\beta}\sum_{n'=0}^{N-1} \begin{pmatrix} \mathbf{G}_N(n-n') & \mathbf{G}_N(n-1-n') \\ \mathbf{G}_N(n+1-n') & \mathbf{G}_N(n-n') \end{pmatrix} \boldsymbol{\beta}^{\mathrm{T}}\mathbf{A}\boldsymbol{\varepsilon}(n'). \tag{31}$$

Due to (3) and (31), the vector of stresses for disordered lattice can be written in terms of the lack of fit as

$$\boldsymbol{\sigma}(n) = E\big(\boldsymbol{\varepsilon}^{(\mathrm{i})}(n) - \boldsymbol{\varepsilon}(n)\big) = \sum_{n'=0}^{N-1} \boldsymbol{\omega}_N(n-n')\boldsymbol{\varepsilon}(n'), \tag{32}$$

where $\boldsymbol{\omega}_N(n-n')$ is the matrix function:

$$\boldsymbol{\omega}_N(n-n') = E^2\mathbf{L}^{-1}\boldsymbol{\beta}\begin{pmatrix} \mathbf{G}_N(n-n') & \mathbf{G}_N(n-1-n') \\ \mathbf{G}_N(n+1-n') & \mathbf{G}_N(n-n') \end{pmatrix} \boldsymbol{\beta}^{\mathrm{T}}\mathbf{A} - E\delta_{n,n'}\mathbf{I}, \tag{33}$$

($\delta_{n,n'}$ is the Kronecker delta and $\mathbf{I}$ is the identity $2R \times 2R$ matrix). This function represents another class of periodic Green's functions: namely, the rth column of $\boldsymbol{\omega}_N(n-n')$ represents *member stresses* in the nth

typical cell, *caused by a unit relative lack of fit* of the rth member in some distant (n')th cell, on a cyclic N-periodic domain.

As follows from (23), each member stress is essentially given by a linear superposition of the lack of fits all around the lattice, where the components of matrix $\boldsymbol{\omega}_N(n-n')$ serve as the coefficients for that superposition. At the same time, when a random variable q is a linear combination of several other random variables $x(n)$ with coefficients $a(n)$,

$$q = \sum_n a(n)x(n), \quad n = 0, 1, \ldots, \tag{34}$$

and all $x(n)$ are independent variables, statistical parameters of the distributions for q and $x(n)$ are simply related:

$$\mu_q = \sum_n a(n)\mu_x(n), \quad s_q^2 = \sum_n a^2(n)s_x^2(n). \tag{35}$$

Here, μ_q, s_q are the mean and standard deviation for q, and $\mu_x(n)$, $s_x(n)$ are means and standard deviations for $x(n)$. Introducing the vectors of means and standard deviation for the member stresses and lacks of fit in the nth typical cell,

$$\begin{aligned} \boldsymbol{\mu}_\sigma(n) &= \begin{pmatrix} \mu_{\sigma_1}(n) & \mu_{\sigma_2}(n) & \ldots \end{pmatrix}^{\mathrm{T}}, \quad \mathbf{s}_\sigma(n) = \begin{pmatrix} s_{\sigma_1}(n) & s_{\sigma_2}(n) & \ldots \end{pmatrix}^{\mathrm{T}}, \\ \boldsymbol{\mu}_\varepsilon(n) &= \begin{pmatrix} \mu_{\varepsilon_1}(n) & \mu_{\varepsilon_2}(n) & \ldots \end{pmatrix}^{\mathrm{T}}, \quad \mathbf{s}_\varepsilon(n) = \begin{pmatrix} s_{\varepsilon_1}(n) & s_{\varepsilon_2}(n) & \ldots \end{pmatrix}^{\mathrm{T}}, \end{aligned} \tag{36}$$

one can write, according to (32) and (35),

$$\boldsymbol{\mu}_\sigma(n) = \mathbf{0}, \quad \mathbf{s}_\sigma(n) = \sqrt{\sum_{n'=0}^{N-1} \boldsymbol{\omega}_N^2(n-n')\mathbf{s}_\varepsilon^2(n')} \tag{37}$$

(the second power and radical notations, here and below in this section, imply taking the corresponding operations over each component of the matrix $\boldsymbol{\omega}_N(n-n')$, vector $\mathbf{s}_\varepsilon(n)$, and the sub-radical vector respectively). This fully describes the normal distributions for the member stresses throughout the lattice.

It is logical to assume that the standard deviation for the lacks of fit, $\mathbf{s}_\varepsilon$ does not depend on the value n:

$$\boldsymbol{\mu}_\sigma(n) = \mathbf{0}, \quad \mathbf{s}_\sigma(n) = \sqrt{\sum_{n'=0}^{N-1} \boldsymbol{\omega}_N^2(n-n')\mathbf{s}_\varepsilon^2}. \tag{38}$$

This situation relates to the case of an absence of a strategy to put, for example, better-fit members in some particular areas of the lattice. It is important to note that $\boldsymbol{\omega}_N^2(n-n')$, similar $\mathbf{G}_N(n-n')$ and $\boldsymbol{\omega}_N(n-n')$, is an N-periodic function of its argument, therefore,

$$\sum_{n'=0}^{N-1} \boldsymbol{\omega}_N^2(n-n') = \sum_{n'=0}^{N-1} \boldsymbol{\omega}_N^2(-n') = \sum_{n'=0}^{N-1} \boldsymbol{\omega}_N^2(n') \tag{39}$$

for any integer n. Thus, we crucially obtain spatial invariance of the sought statistics on the cyclic domains:

$$\boldsymbol{\mu}_\sigma = \mathbf{0}, \quad \mathbf{s}_\sigma = \sqrt{\sum_{n=0}^{N-1} \boldsymbol{\omega}_N^2(n)\mathbf{s}_\varepsilon^2}. \tag{40}$$

In practice, this implies that within the periodic Born-von Kármán model, the standard deviations have to be calculated for a small number of members in one typical cell only, instead of possibly thousands of bars in an entire lattice.

3.2. Plate-like problem

For the plate-like case, the (n,m)th typical cell is normally confined between four nodal locations (n,m), $(n+1,m)$, $(n,m+1)$ and $(n+1,m+1)$—see Figs. 4c and 5c. Then, using arguments similar to (26)–(33)), we obtain the two-dimensional Green's function for the initial stress in the form:

$$\boldsymbol{\omega}_{N,M}(n,m) = E^2\mathbf{L}^{-1}\boldsymbol{\beta}\times\begin{pmatrix} \mathbf{G}_{N,M}(n,m) & \mathbf{G}_{N,M}(n-1,m) & \mathbf{G}_{N,M}(n,m-1) & \mathbf{G}_{N,M}(n-1,m-1) \\ \mathbf{G}_{N,M}(n+1,m) & \mathbf{G}_{N,M}(n,m) & \mathbf{G}_{N,M}(n+1,m-1) & \mathbf{G}_{N,M}(n,m-1) \\ \mathbf{G}_{N,M}(n,m+1) & \mathbf{G}_{N,M}(n-1,m+1) & \mathbf{G}_{N,M}(n,m) & \mathbf{G}_{N,M}(n-1,m) \\ \mathbf{G}_{N,M}(n+1,m+1) & \mathbf{G}_{N,M}(n,m+1) & \mathbf{G}_{N,M}(n+1,m) & \mathbf{G}_{N,M}(n,m) \end{pmatrix} \times \boldsymbol{\beta}^{\mathrm{T}}\mathbf{A} - E\delta_{n,0}\delta_{m,0}\mathbf{I}. \tag{41}$$

Here, $\boldsymbol{\beta}, \mathbf{L}$ and $\mathbf{A}$ are similarly the connectivity matrix, diagonal matrices of perfect member lengths and cross-section areas for the bars of a typical cell, and $\mathbf{G}_{N,M}(n,m)$ is a two-dimensional displacement Green's function (23).

Finally, the statistical parameters of distributions for the initial member stresses on a double cyclic domain are

$$\boldsymbol{\mu}_\sigma = \mathbf{0}, \quad \mathbf{s}_\sigma = \sqrt{\sum_{n=0}^{N-1}\sum_{m=0}^{M-1}\boldsymbol{\omega}^2_{N,M}(n,m)\mathbf{s}^2_\varepsilon}, \tag{42}$$

where the components of vectors $\boldsymbol{\mu}_\sigma$, $\mathbf{s}_\sigma$ are means and standard deviations for the stress in typical members at arbitrary spatial locations, and $\mathbf{s}_\varepsilon$ is the given standard deviation for the relative lack of fit of such members.

4. Illustrative examples

Example 1. Consider the chain of an arbitrary number N of elastic elements, supported as shown in Fig. 3. Assume the structure is free of external loads. The distance between the left and right support is deterministic, and equal to NL, where L is the perfect length of the elements. However, the members do not match this perfect length in a random way, due to temperature gradients or manufacture's tolerance. The relative lack of fit ε of the disassembled elements is given by the standard deviation s_ε, and one seeks to find the distribution for the initial stresses after assembling the structure.

This type of fixtures is an example of Born-von Kármán boundary conditions. They assure the same (trivial) boundary displacements, and the zero resultant of end support reactions. Thus, the structure is a topological ring (with nodes $n=0$ and $n=N$ formally merged), and the approach presented in Section 3.1 will yield an analytically exact solution to this problem. The values of the stiffness operator's kernel function give, for this lattice,

$$\mathbf{K}(-1) = \mathbf{K}(1) = -\frac{EA}{L}, \quad \mathbf{K}(0) = 2\frac{EA}{L}. \tag{43}$$

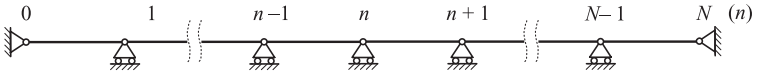

Fig. 3. Chain of N elastic elements.

The N-periodic displacement Green's function can be then constructed according to Eq. (19). The Fourier image $\widetilde{\mathbf{K}}_N(p)$ is here the scalar quantity,

$$\widetilde{\mathbf{K}}_N(p) = \frac{EA}{L}\left(-\exp\left(-\mathrm{i}2\pi p\frac{n}{N}\right) + 2 - \exp\left(\mathrm{i}2\pi p\frac{n}{N}\right)\right) = \frac{4EA}{L}\sin^2\left(\frac{p\pi}{N}\right), \tag{44}$$

so that we obtain

$$\mathbf{G}_N(n) = \frac{1}{N}\sum_{p=1}^{N-1}\widetilde{\mathbf{K}}_N^{-1}(p)\exp\left(\mathrm{i}2\pi p\frac{n}{N}\right) = \frac{L}{4EAN}\sum_{p=1}^{N-1}\csc^2\left(\frac{p\pi}{N}\right)\exp\left(\mathrm{i}2\pi p\frac{n}{N}\right). \tag{45}$$

The typical cell for this lattice is represented by a single member, for whom the connection matrix acquires the form

$$\boldsymbol{\beta} = (-1 \quad 1). \tag{46}$$

Utilising (45) and (46), construct the initial stress Green's function, according to (33), employing also $\mathbf{L} \equiv L$ and $\mathbf{A} \equiv A$,

$$\begin{aligned}\boldsymbol{\omega}_N(n) &= \frac{E^2A}{L}\boldsymbol{\beta}\begin{pmatrix}\mathbf{G}_N(n) & \mathbf{G}_N(n-1)\\ \mathbf{G}_N(n+1) & \mathbf{G}_N(n)\end{pmatrix}\boldsymbol{\beta}^{\mathrm{T}} - E\delta_{n,0}\\ &= \frac{E}{4N}\left(-\sum_{p=1}^{N-1}\csc^2\left(\frac{p\pi}{N}\right)\exp\left(\mathrm{i}2\pi p\frac{n-1}{N}\right) + 2\sum_{p=1}^{N-1}\csc^2\left(\frac{p\pi}{N}\right)\exp\left(\mathrm{i}2\pi p\frac{n}{N}\right)\right.\\ &\quad\left. - \sum_{p=1}^{N-1}\csc^2\left(\frac{p\pi}{N}\right)\exp\left(\mathrm{i}2\pi p\frac{n+1}{N}\right)\right) - E\delta_{n,0}.\end{aligned} \tag{47}$$

This can be simplified as the following:

$$\begin{aligned}\boldsymbol{\omega}_N(n) &= \frac{E}{4N}\sum_{p=1}^{N-1}\csc^2\left(\frac{p\pi}{N}\right)\left(-\exp\left(\mathrm{i}2\pi p\frac{n-1}{N}\right) + 2\exp\left(\mathrm{i}2\pi p\frac{n}{N}\right) - \exp\left(\mathrm{i}2\pi p\frac{n+1}{N}\right)\right) - E\delta_{n,0}\\ &= \frac{E}{N}\sum_{p=1}^{N-1}\csc^2\left(\frac{p\pi}{N}\right)\sin^2\left(\frac{p\pi}{N}\right)\exp\left(\mathrm{i}2\pi p\frac{n}{N}\right) - E\delta_{n,0} = \frac{E}{N}\sum_{p=1}^{N-1}\exp\left(\mathrm{i}2\pi p\frac{n}{N}\right) - E\delta_{n,0}.\end{aligned} \tag{48}$$

Add and subtract the term E/N to obtain the entire period summation in (48), and to further simplify as

$$\boldsymbol{\omega}_N(n) = E\left(\frac{1}{N}\sum_{p=0}^{N-1}\exp\left(\mathrm{i}2\pi p\frac{n}{N}\right) - \frac{1}{N} - \delta_{n,0}\right) = E\left(\delta_{n,0} - \frac{1}{N} - \delta_{n,0}\right) = -\frac{E}{N}. \tag{49}$$

Importantly, the stress Green's function (49) reads a constant quantity for all n. This physically implies that the initial member stress does not depend on the distance from the element where it is measured to the element, whose lack of fit causes this stress. In other words, whatever particular (deterministic) lacks of fit are imposed, the value of the corresponding initial stress will be the same throughout the lattice.

Finally, the sought standard deviation can be found according to (40):

$$s_\sigma = \sqrt{\sum_{n=0}^{N-1}\boldsymbol{\omega}_N^2(n)s_\varepsilon^2} = s_\varepsilon\sqrt{\sum_{n=0}^{N-1}\frac{E^2}{N^2}} = s_\varepsilon\sqrt{\frac{E^2}{N}} = \frac{Es_\varepsilon}{\sqrt{N}}. \tag{50}$$

The distribution for stresses will logically become narrower when the total number of chain elements is growing. For an infinite chain, $N \to \infty$, any finite lack of fit produces zero initial member stress.

Noteworthy, the same result can be also obtained from elementary arguments. Indeed, if the sequence $\varepsilon(n) = \Delta L(n)/L$, $n = 0, 1, \ldots, N-1$ gives a particular realization for the members' lacks of fit, the initial stress can be written for a chain of N elements, as

$$\sigma = \frac{E}{N}\sum_{n=0}^{N-1}\varepsilon(n). \tag{51}$$

Here, we *initially* presumed its invariance throughout the structure, due to the specified means of support. Since all $\varepsilon(n)$ are independent random values with the same standard deviation s_ε, formulas (35) and (51) can be directly used to give s_σ as (50). This lends support to the validity of the present approach. For more complicated structures, with a varying stress Green's function, such elementary arguments cannot be normally found. Then the sums of (40) or (42) have to be evaluated directly for particular material properties and values N, M, and if required, the results can be verified by Monte–Carlo simulations, as in the next examples.

Example 2. Assume there are applied cyclic boundary conditions on the X-braced planar grid depicted in Fig. 4, there exist random imperfections of the members' ideal lengths described by the relative parameter $\varepsilon = \Delta L/L$. The probability distribution for ε is normal, with a zero mean and the same standard deviation s_ε for all members. One seeks to evaluate the parameters of initial stress distribution for all four types of structural elements, shown on Fig. 4c.

On putting the lengths of vertical, horizontal and diagonal bars to be L, $\sqrt{3}L$ and $2L$ respectively, and E, A as the Young's modulus and cross-sectional areas of all bars, the lattice associate substructure, Fig. 4b, provides the following values of the stiffness kernel function:

$$\begin{aligned}
&\mathbf{K}(0,-1) = \mathbf{K}(0,1) = -\frac{EA}{L}\begin{pmatrix} 0 & 0 \\ 0 & 1 \end{pmatrix}, \quad \mathbf{K}(-1,0) = \mathbf{K}(1,0) = -\frac{EA}{\sqrt{3}L}\begin{pmatrix} 1 & 0 \\ 0 & 0 \end{pmatrix}, \\
&\mathbf{K}(-1,-1) = \mathbf{K}(1,1) = -\frac{EA}{8L}\begin{pmatrix} 3 & \sqrt{3} \\ \sqrt{3} & 1 \end{pmatrix}, \quad \mathbf{K}(-1,1) = \mathbf{K}(1,-1) = -\frac{EA}{8L}\begin{pmatrix} 3 & -\sqrt{3} \\ -\sqrt{3} & 1 \end{pmatrix}, \\
&\mathbf{K}(0,0) = \frac{EA}{24L}\begin{pmatrix} 4(9+4\sqrt{3}) & 0 \\ 0 & 60 \end{pmatrix}.
\end{aligned} \tag{52}$$

The geometry of a cell comprised of the four typical members, Fig. 4c, implies the connection matrix, along with the matrices of members' lengths and cross-sectional areas, of the forms:

$$\boldsymbol{\beta} = \frac{1}{2}\begin{pmatrix} 0 & -2 & 0 & 0 & 0 & 2 & 0 & 0 \\ -2 & 0 & 2 & 0 & 0 & 0 & 0 & 0 \\ -\sqrt{3} & -1 & 0 & 0 & 0 & 0 & \sqrt{3} & 1 \\ 0 & 0 & \sqrt{3} & -1 & -\sqrt{3} & 1 & 0 & 0 \end{pmatrix}, \quad \mathbf{L} = L\begin{pmatrix} 1 & 0 & 0 & 0 \\ 0 & \sqrt{3} & 0 & 0 \\ 0 & 0 & 2 & 0 \\ 0 & 0 & 0 & 2 \end{pmatrix}, \quad \mathbf{A} = A\begin{pmatrix} 1 & 0 & 0 & 0 \\ 0 & 1 & 0 & 0 \\ 0 & 0 & 1 & 0 \\ 0 & 0 & 0 & 1 \end{pmatrix}. \tag{53}$$

Next, construct the displacement Green's function according to Eq. (23):

$$\mathbf{G}_{5,5}(n,m) = \frac{1}{25}\sum_{p=0}^{4}\sum_{q=0}^{4}\widetilde{\mathbf{G}}_{5,5}(p,q)\exp\left(-\mathrm{i}\frac{2\pi}{5}(pn+qm)\right), \quad \widetilde{\mathbf{G}}_{5,5}(p,q) = \begin{cases} \widetilde{\mathbf{K}}_{5,5}^{-1}(p,q), & p+q>0, \\ \mathbf{0}, & p=q=0. \end{cases} \tag{54}$$

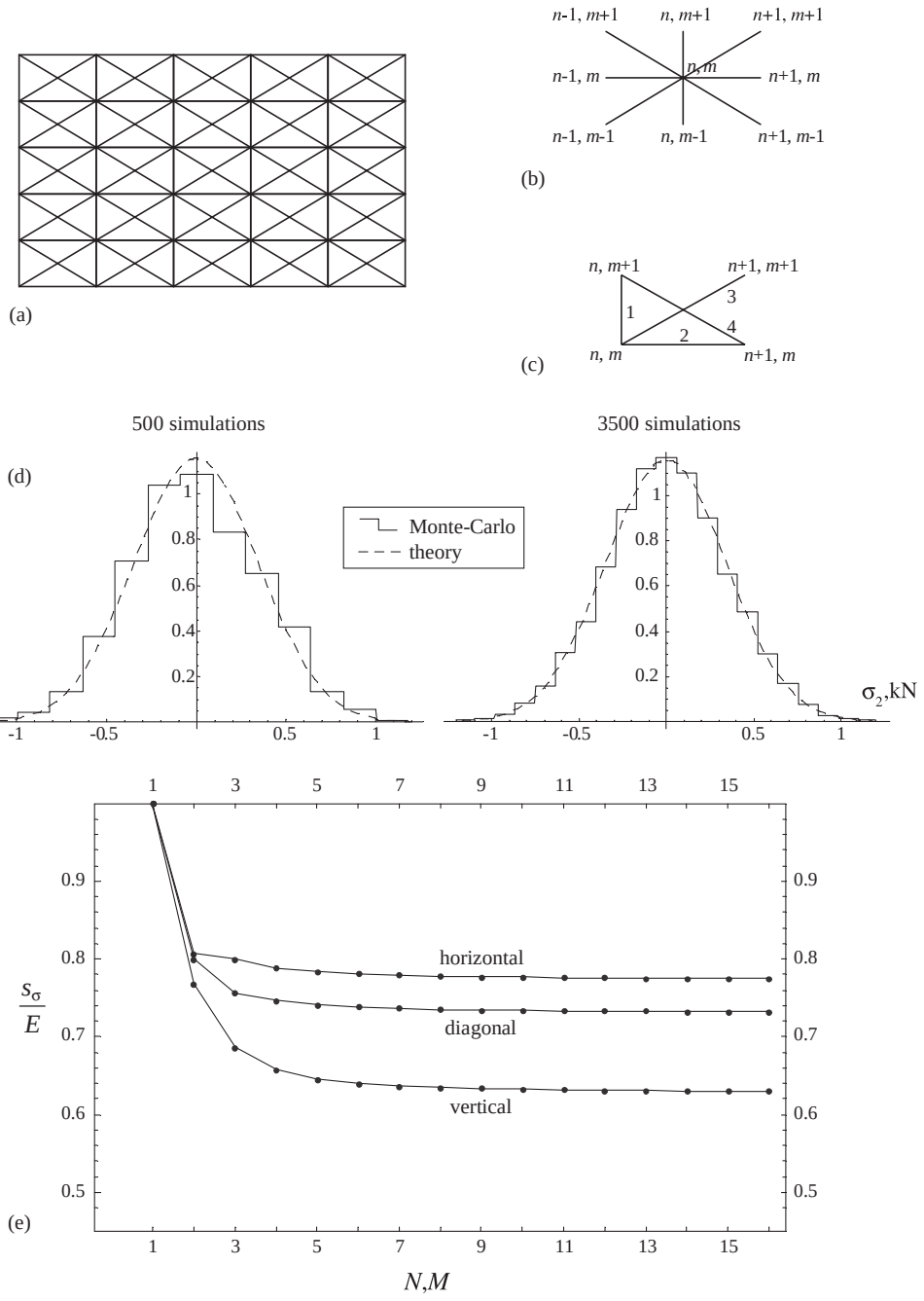

Fig. 4. X-braced planar grid (a); associate substructure (b), numbering of members within a typical cell (c). Probability density for the horizontal member stress (d), $E = 2 \times 10^5$ N/mm^2, $s_\varepsilon = 0.0022$. Dependence of standard deviations for member stresses on the lattice size (e).

Here, the zero harmonic $\widetilde{\mathbf{G}}_{5,5}(0,0)$ of the Green's function is trivial, because

$$\widetilde{\mathbf{K}}_{5,5}(0,0) = \sum_{n=-1}^{1} \sum_{m=-1}^{1} \mathbf{K}(n,m) = \mathbf{0} \tag{55}$$

for this structure, i.e. it has no eigenvalues other than zero. The Fourier image of the kernel function can be sought as Eq. (24) and, by employing the symmetry $\mathbf{K}(-n,-m)=\mathbf{K}(n,m)$ see (52), rearranged to give

$$\begin{aligned}
&\widetilde{\mathbf{K}}_{5,5}(p,q)\\
&=\sum_{n=-1}^{1}\sum_{m=-1}^{1}\mathbf{K}(n,m)\exp\left(-\mathrm{i}\frac{2\pi}{5}(pn+qm)\right)\\
&=-4\big(\mathbf{K}(1,0)\sin^2(w_p)+\mathbf{K}(0,1)\sin^2(w_q)+\mathbf{K}(1,1)\sin^2(w_p+w_q)+\mathbf{K}(1,-1)\sin^2(w_p-w_q)\big)\\
&=\frac{EA}{6L}\begin{pmatrix}8\sqrt{3}\sin^2(w_p)+\sin^2(w_p+w_q)+9\sin^2(w_p-w_q) & 3\sqrt{3}\sin(2w_p)\sin(2w_q)\\ 3\sqrt{3}\sin(2w_p)\sin(2w_q) & 3(8\sin^2(w_q)+\sin^2(w_p+w_q)+\sin^2(w_p-w_q))\end{pmatrix},
\end{aligned}\tag{56}$$

where $w_p=\pi pn/5$, $w_q=\pi qn/5$.

The required values of the stress Green's function $\boldsymbol{\omega}_{5,5}(n,m)$, $n=0,1,\ldots,4$, $m=0,1,\ldots,4$, can then be found using (41) and (53). Then we can use (42) to express the sought standard deviations for initial stress in four typical members through the Young's modulus and value s_ε only:

$$\mathbf{s}_\sigma\equiv\begin{pmatrix}s_{\sigma_1}\\ s_{\sigma_2}\\ s_{\sigma_3}\\ s_{\sigma_4}\end{pmatrix}=s_\varepsilon\sqrt{\sum_{n=0}^{4}\sum_{m=0}^{4}\boldsymbol{\omega}_{5,5}^2(n,m)\begin{pmatrix}1\\1\\1\\1\end{pmatrix}}=Es_\varepsilon\begin{pmatrix}0.64531\\0.78412\\0.74108\\0.74108\end{pmatrix}\tag{57}$$

(the statistics appeared invariant with respect to the values L and A). Here, parameter s_ε is taken outside the radical sign, since it reads the same value for all element types in the present problem statement. Thus, larger initial stresses are expected in horizontal bars, and smaller—in the vertical bars. Logically, stresses in the left and right diagonal members show a similar distribution; this is determined by the mirror symmetry of the lattice in relation to a medial line.

This result was verified with numerical Monte–Carlo simulations, where the lack of fit was modelled through the use of El-Sheikh technique, Fig. 1. The bars' lengths were taken as a random, normally distributed sample with standard deviation $s_\varepsilon=0.0022$ for the relative lack of fit $\varepsilon=\Delta L/L$; the Young's modulus was 200 kN/mm^2. For a given sample, the nodal forces were evaluated as explained in Fig. 1, and displacements—by solving the global stiffness matrix equation $\mathbf{Kd}=\mathbf{f}$ with periodic (cyclic) boundary conditions. The initial stress was found after calculating the strain (3), for the four typical members, Fig. 4c. For each next sample of imperfections, the stress was found for the same set of bars, until the sought statistics emerged. First, 500 simulations of this kind were accomplished to give $Q=500$ random stresses for a typical member, whose mean standard deviation was calculated conventionally as

$$\mu_\sigma=\frac{1}{Q}\sum_{k=1}^{Q}\sigma^{(k)},\quad s_\sigma=\sqrt{\frac{1}{Q-1}\sum_{k=1}^{Q}(\sigma^{(k)}-\mu_\sigma)^2}.\tag{58}$$

The results obtained were very close to the theoretical predictions, and additional simulations further verified convergence of the analytical and numerical values. This can be seen from Table 1, and also from Fig. 4d, where the theoretical and numerical probability density functions are shown to converge with the growth of Q.

Using the analytical arguments similar to (54)–(57), one can easily evaluate the statistics of stress for other related lattices. Of particular interest is to investigate its behaviour with the change of lattice size parameters N, M. Such a study was undertaken over the range $N=M=1,2,\ldots,16$; the results are presented graphically in Fig. 4e. Remarkably, with the growth of N, M, the standard deviations do not tend to

Table 1
Means and standard deviations for initial stress (N/mm^2) in typical members

	Vertical	Horizontal	Right diagonal	Left diagonal
$Q = 500$	15.04, 287.4	3.968, 343.1	−10.84, 322.0	−9.742, 330.5
$Q = 3500$	2.322, 284.1	5.875, 344.4	5.109, 327.2	−1.296, 324.94
Theory	**0, 283.9**	**0, 345.0**	**0, 326.1**	**0, 326.1**

zeros, in contrast to the case of elastic chain (50). The reason for that is the following: the chain structure becomes statically determinate in the hypothetical infinite limit $N \to \infty$, when the right end reaction vanishes. However, the X-braced grid remains indeterminate for the entire range of N, M, including the infinite limit, due to the redundancy of its individual constituent blocks, for example, the single X-braced rectangular cells shown Fig. 6a. Thus, with the growth of lattice sizes, the standard deviations for initial member stresses asymptotically approach some finite non-trivial values that should be typical for all large lattices, when the boundary effects diminish.

Example 3. Finally, investigate what changes to the obtained distributions can be caused by removing some redundant elements from the lattice considered in Example 2. For instance, consider removal of the left diagonal members, Fig. 5a. The associate substructure for the new lattice is shown in Fig. 5b, so that the values of stiffness kernel function become

$$\begin{aligned}
&\mathbf{K}(0,-1) = \mathbf{K}(0,1) = -\frac{EA}{L}\begin{pmatrix} 0 & 0 \\ 0 & 1 \end{pmatrix}, \quad \mathbf{K}(-1,0) = \mathbf{K}(1,0) = -\frac{EA}{\sqrt{3}L}\begin{pmatrix} 1 & 0 \\ 0 & 0 \end{pmatrix}, \\
&\mathbf{K}(-1,-1) = \mathbf{K}(1,1) = -\frac{EA}{8L}\begin{pmatrix} 3 & \sqrt{3} \\ \sqrt{3} & 1 \end{pmatrix}, \quad \mathbf{K}(-1,1) = \mathbf{K}(1,-1) = \mathbf{0}, \\
&\mathbf{K}(0,0) = \frac{EA}{12L}\begin{pmatrix} 9+8\sqrt{3} & 3\sqrt{3} \\ 3\sqrt{3} & 27 \end{pmatrix},
\end{aligned} \tag{59}$$

and the displacement Green's functions simplifies to

$$\begin{aligned}
&\mathbf{G}_{5,5}(n,m) = \frac{1}{25}\sum_{p=0}^{4}\sum_{q=0}^{4}\widetilde{\mathbf{G}}_{5,5}(p,q)\exp\left(-\mathrm{i}\frac{2\pi}{5}(pn+qm)\right), \quad \widetilde{\mathbf{G}}_{5,5}(p,q) = \begin{cases} \widetilde{\mathbf{K}}_{5,5}^{-1}(p,q), & p+q>0, \\ \mathbf{0}, & p=q=0, \end{cases} \\
&\widetilde{\mathbf{K}}_{5,5}(p,q) = \frac{EA}{6L}\begin{pmatrix} 8\sqrt{3}\sin^2(w_p)+9\sin^2(w_p+w_q) & 3\sqrt{3}\sin^2(w_p+w_q) \\ 3\sqrt{3}\sin^2(w_p+w_q) & 3(8\sin^2(w_q)+\sin^2(w_p+w_q)) \end{pmatrix}.
\end{aligned} \tag{60}$$

The connectivity matrix, matrices of members' lengths and cross-section areas for the pattern of three typical members, Fig. 5c, become

$$\boldsymbol{\beta} = \frac{1}{2}\begin{pmatrix} 0 & -2 & 0 & 0 & 0 & 2 & 0 & 0 \\ -2 & 0 & 2 & 0 & 0 & 0 & 0 & 0 \\ -\sqrt{3} & -1 & 0 & 0 & 0 & 0 & \sqrt{3} & 1 \end{pmatrix}, \quad \mathbf{L} = L\begin{pmatrix} 1 & 0 & 0 \\ 0 & \sqrt{3} & 0 \\ 0 & 0 & 2 \end{pmatrix}, \quad \mathbf{A} = A\begin{pmatrix} 1 & 0 & 0 \\ 0 & 1 & 0 \\ 0 & 0 & 1 \end{pmatrix}. \tag{61}$$

Expressions (60) and (61) provide one with all necessary information for calculating the values of stress Green's function (41). Employing them for (42), we obtain the following standard deviations for the initial stress in typical elements:

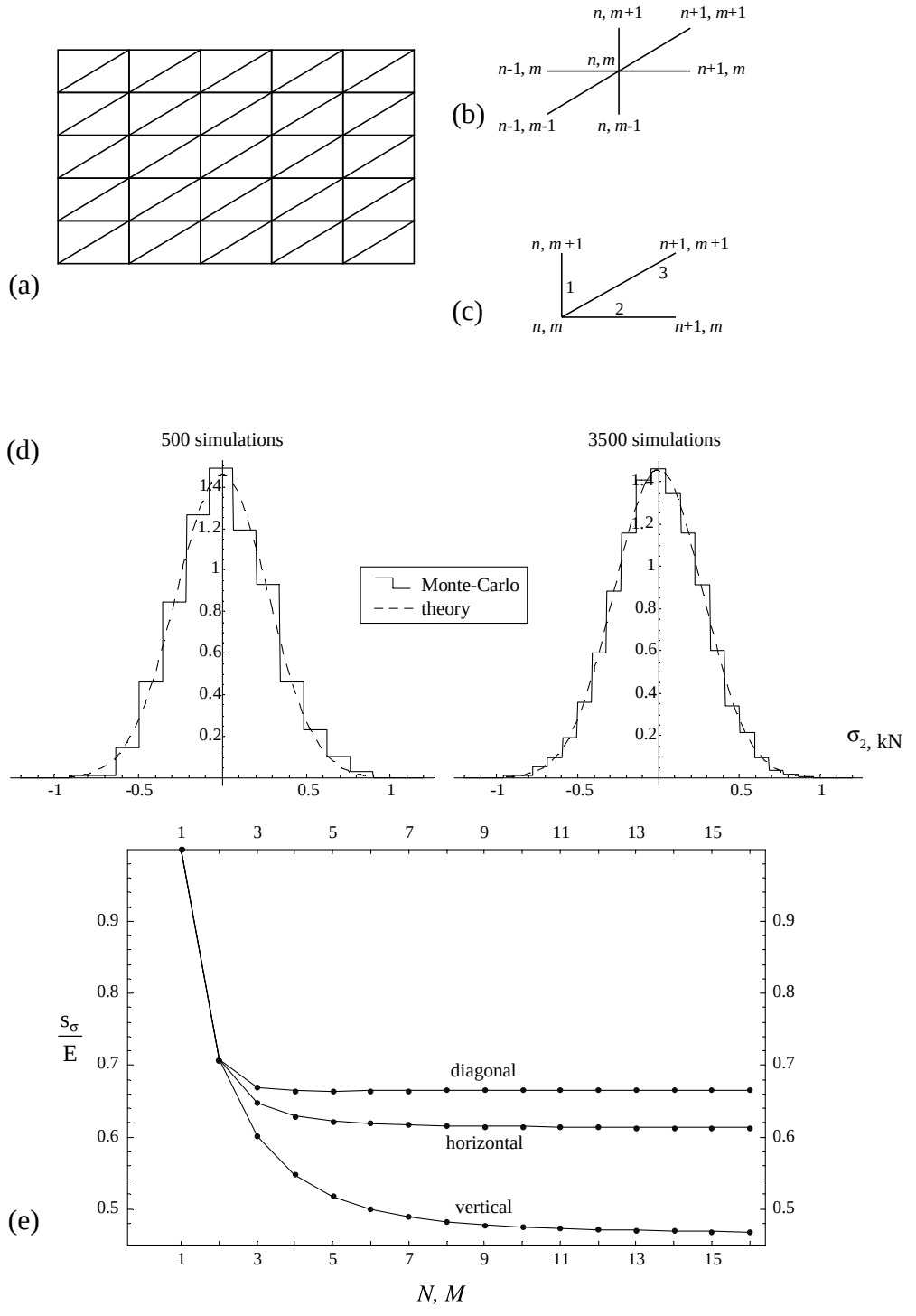

Fig. 5. Probability density for the horizontal member stress (d), $E = 2 \times 10^5$ N/mm^2, $s_\varepsilon = 0.0022$, and behaviour of standard deviations (e) after the left diagonal member removal (a–c).

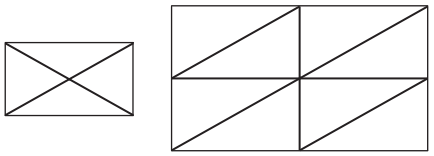

(a) (b)

Fig. 6. Redundant constituent units for the original X-braced grid (a), and after the left diagonal member removal (b); the edge bars are formally split along to halve the cross-section areas.

$$\mathbf{s}_\sigma \equiv \begin{pmatrix} s_{\sigma_1} \\ s_{\sigma_2} \\ s_{\sigma_3} \end{pmatrix} = s_\varepsilon \sqrt{\sum_{n=0}^{4}\sum_{m=0}^{4} \boldsymbol{\omega}_{5,5}^2(n,m) \begin{pmatrix} 1 \\ 1 \\ 1 \end{pmatrix}} = E s_\varepsilon \begin{pmatrix} 0.51762 \\ 0.62212 \\ 0.66409 \end{pmatrix}. \tag{62}$$

Here, it was similarly assumed that the standard deviation for the relative lack of fit, s_ε, is the same for all members.

In accordance with (62), the probability distributions for initial member stresses are narrower, when compared with the corresponding results for the X-braced lattice (57). The analytical data (62) were similarly verified with a series of numerical Monte–Carlo simulations. The theoretical and numerical results are in good agreement. Their convergence with the growth of number of calculation is depicted in Fig. 5d for the horizontal members.

Although the single rectangular cell with one diagonal is a non-redundant structure, the behaviour of the standard deviations with the change of N, M, Fig. 5e, is similar to the previous case shown in Fig. 4e. When $N, M \to \infty$, these parameters asymptotically tend to some fixed finite values, so that no decay to the zero level, as in (50), appears. We can attribute this phenomenon to the presence of a larger redundant constituent unit for this structure, depicted in Fig. 6b.

5. Concluding remarks

In this paper, an analytical approach for studying initial member stress in regular lattice structures with geometrical imperfections has been presented. Solutions to benchmark problems have been verified through direct Monte–Carlo simulation. The study of particular example structures indicates that the initial member stress can be diminished substantially with the members redundancy decrease. However, the effect will reveal itself in all cases, when the lattice features a redundant constituent block, even if the latter is comprised of several typical cells.

The periodic boundary model considered provides a reliable approximation for large realistic problems. Importantly, it yields higher values for the standard deviations in studying smaller lattices, compared with those for $N, M \to \infty$ (Figs. 4e and 5e). Hence the use of this approximation will not lead to underestimation of this dangerous phenomenon in realistic finite structures, and in the analysis of edge clamped lattices it will provide one with almost exact solutions. Besides, the obvious computational effectiveness of the approach, compared with numerical techniques is another important advantage. For most problems the cost of analytical evaluation of the statistical parameters with the use of (40) or (42) is not more than the cost of one random lattice simulation. This implies savings in CPU effort up to 10^3–10^4 times, compared with numerical Monte–Carlo simulations, when reliable estimates are sought.

The asymptotical behaviour of the standard deviations in the limit $N, M \to \infty$ is particularly remarkable, and its further analysis is planned. The approach can be also modified for studying residual stress in disordered crystal lattices.

Acknowledgement

This research was supported by the National Science Foundation.

References

Affan, A., Calladine, C.R., 1989. Initial bar tensions in pin-jointed assembles. International Journal of Space Structures 4 (1), 1–16.

El-Sheikh, A.I., 1995. Sensitivity of space trusses to member geometric imperfections. International Journal of Space Structures 10 (2), 89–98.

El-Sheikh, A.I., 1997. Effect of member length imperfection on triple-layer space trusses. Engineering Structures 19 (7), 540–550.

Karpov, E.G., Stephen, N.G., Dorofeev, D.L., 2002. On static analysis of finite repetitive structures by discrete Fourier transform. International Journal of Solids and Structures 39 (16), 4291–4310.

Keane, A.J., Price, W.G., 1989. On the vibrations of mono-coupled periodic and near-periodic structures. Journal of Sound and Vibrations 128 (3), 423–450.

Langley, R.S., 1994. One-parameter scaling in weakly disordered one-dimensional systems. Journal of Physics—Condensed Matter 6 (40), 8259–8268.

Li, D., Benaroya, H., 1992. Dynamics of periodic and near-periodic structures. Applied Mechanics Reviews 45 (11), 447–460.

Lin, Y.K., 1996. Dynamics of disordered periodic structures. Applied Mechanics Reviews 49 (2), 57–64.

Schmidt, L.C., Morgan, P.R., Clarkson, J.A., 1976. Space trusses with brittle-type strut buckling. Journal of the Structural Division, ASCE 102 (7), 1479–1492.

Schmidt, L.C., Morgan, P.R., Gregg, B.M., 1983. Correlation study of ultimate load capacities of space trusses. In: Morris, L.J. (Ed.), Instability and Plastic Collapse of Steel Structures. Granada, London, pp. 195–204.

Smith, E.A., Epstein, H.I., 1980. Hartford Coliseum roof collapse: structural collapse sequence and lessons learned. Civil Engineering, ASCE 50, 59–62.

Thornton, C.H., Lew, P., 1984. Investigation of the causes of Hartford Coliseum collapse. In: Nooshin, H. (Ed.), Proceedings of the 3rd International Conference on Space Structures. Elsevier Applied Science Publishers, pp. 636–641.